Graphical Abstract

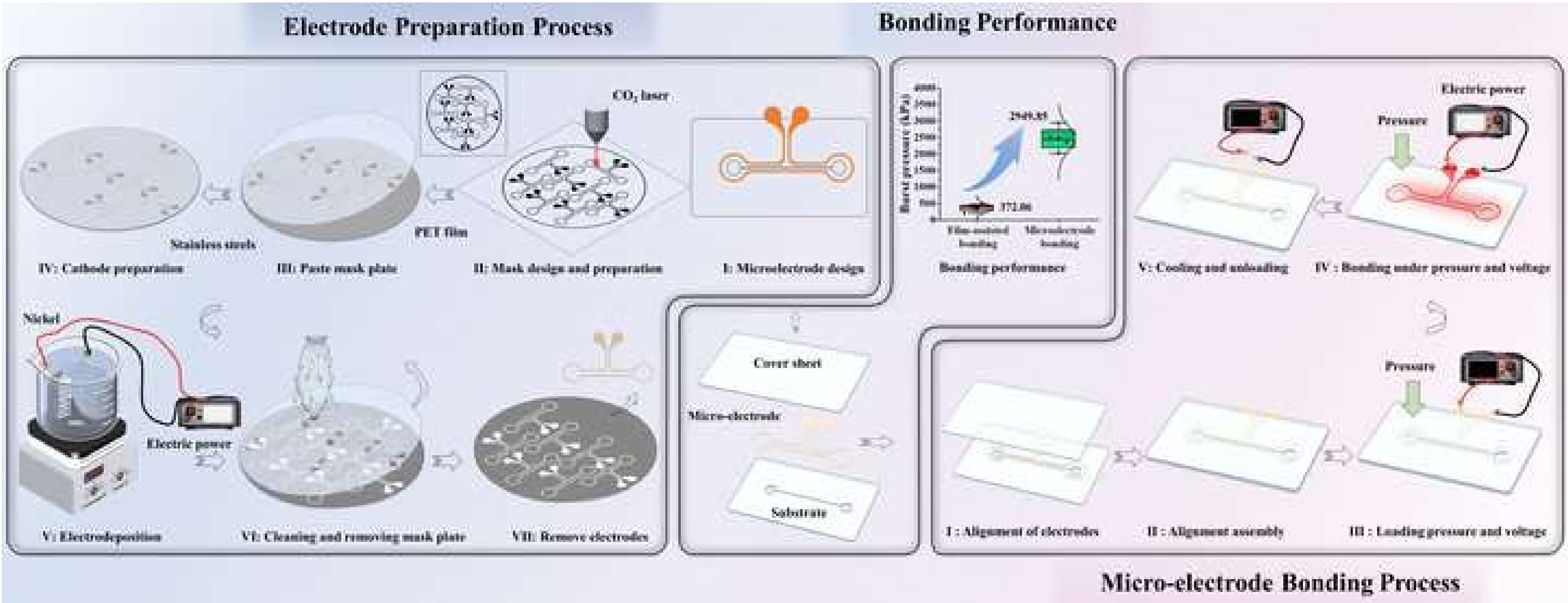

Highlights

1. A microelectrode bonding technology for microfluidic chips is engineered.

2. Microelectrode bonding achieves sub-3V rapid sealing in 15 seconds.

3. Burst pressures exceed 2.9 MPa with minimal microchannel deformation.

4. Technology is green and uses no hazardous chemicals or produces pollutants.

5. Adaptability to various materials broadens application scope.

An innovative patternable microelectrode bonding technology for high-performance and cost-effective sealing in microfluidic chips

Baishun Zhao[a], Dimitrios Kontziampasis[b c d], Lei Huang [a], Wangqing Wu(吴旺青)[* a c], Bingyan Jiang[a]

a. State Key Laboratory of Precision Manufacturing for Extreme Service Performance, School of Mechanical and Electrical Engineering, Central South University, Changsha 410083, China

b. Mechanical and Industrial Engineering, School of Science and Engineering, University of Dundee, DD1 4HN, Dundee, Scotland, UK

c. Dundee International Institute of Central South University, Central South University, 410083 Changsha, China

d. School of Mechanical Engineering, Faculty of Science and Engineering, The University of Leeds, LS2 9JT, Leeds, UK

*Corresponding author E-mail address: csuwwq@csu.edu.cn (Wangqing Wu)

ORCID: B. Zhao: 0000-0001-7530-8630, D. Kontziampasis: 0000-0002-6787-8892, W. Wu: 0000-0002-8384-9012, B. Jiang: 0000-0002-5548-3340

Abstract

Microfluidic chips pose as an interdisciplinary frontier as they integrate various fields, while typically serving as a novel technological platform for precise manipulation of minute liquid volumes and biological analysis. However, the chase for enhanced bonding quality in order to fabricate these chips correctly, has led to the use of increasingly complex technology, limiting the marketability of microfluidic products. In this work, a novel microelectrode bonding technology is proposed, which addresses the demands for reliable, low-cost, and high-throughput bonding. The proposed process utilizes the Joule heating effect of microelectrodes at low voltages, in order to rapidly generate sufficient heat and allow for the successful bonding of the chip. The material used for the microelectrodes is nickel, and the method chosen for their fabrication is small-batch electrodeposition. The microelectrodes and microchannels morphology are characterized by Extended Depth of Field Microscopy, while the quality of heating produced is assessed by a high-speed infrared camera. The finalized bonding strength is characterized by measuring the microchannel burst pressure, using an apparatus comprising of a syringe pump, a precision pressure gauge, and a connecting tubing. The results prove that this is a rapid polymer bonding method, which uses less than 3 Volts. Additionally, the results underscore the process's effectiveness, yielding chips with burst strengths over 2.9 MPa, while microchannel deformations are kept under 10%. Finally, the advantages of the technology are discussed and its limitations are eliminated by further conceptualization. The proposed method uses no chemicals or contaminants,

nor complex equipment, rendering it simple, green, and sustainable. This paves the way for the development of new efficient and greener paradigms, aiming towards leading engineering and manufacturing to a sustainable future.

Keywords: Microfluidics; Microfabrication; Bonding technology; Polymers; Sealing; Microelectrode bonding

1 Introduction

Microfluidic technology has emerged as a pivotal advancement in the biomedical and chemical analysis sectors, and is epitomized by microfluidic chips [1–3]. A microfluidic chip is a miniature device that integrates microchannel networks and micro-mechanical structures, designed for precise control of the movement and reactions of minute amounts of fluids and particles at the micrometer scale [4,5]. These devices integrate micro-nano technology with biomedical sciences, and offer numerous advantages, i.e. high efficiency [6–8], precision and control [9,10], miniaturization [11], and the capacity for complex analyses and syntheses [12,13] on a single platform [14,15]. Applications span from drug delivery systems and diagnostic assays, to environmental monitoring and lab-on-chip devices, demonstrating their versatility and significance in advancing biomedical, and analytical research [16,17].

Nowadays, microfluidic technology has reached its maturity stage, with a substantial number of devices successfully transitioning from prototypes to commercialized products [10,18]. Typically, the production of microfluidic chips involves intricate and critical processes regarding design, verification, manufacturing, which include bonding. The marketization and widespread adoption of microfluidics is however dependent on the further development and the standardization of efficient and reliable bonding technologies to improve the sustainability of the field [19]. At this stage, there is a pressing need for reliable, cost-effective, and high-volume thermoplastic bonding methods with improved sustainability. For polymetric microfluidics, polydimethylsiloxane (PDMS) and thermoplastic are the two major materials, and both materials present their own unique qualities in microfluidic applications [18]. Plasma bonding is typically suitable for the design and validation phases of lab-scale hybrid microfluidic devices composed of PDMS and glass [20]. In hybrid PDMS/glass microfluidic devices, surface hydroxylation via oxygen plasma treatment, ultraviolet-ozone (UVO) treatment, or corona discharge method is the main bonding technique. However, the use of plasma systems for thermoplastic polymers usually leads to very weak bonding [21]. Moreover, UV exposure, ozone or oxygen plasma for thermoplastic polymers has the ability to produce cytotoxic by-products, as for example hydrogen peroxide, which must be avoided in most biomedical applications and cell studies [22].

Traditional methods for thermoplastic, i.e. adhesive bonding [23,24], solvent bonding [25,26], thermal bonding [27,28], chemical bonding [29], as well as laser [30,31], and ultrasonic welding [32,33], provide solutions for numerous material and application requirements. However, all these methods appear to possess respective advantages and drawbacks [21].

The use of adhesive layers provides a rapid technology that preserves transparency, allows permeability for cell culturing applications and pre-functionalization, but typically faces cytotoxicity and adsorption challenges, as well as channel thickness limitations for double-sided layers [5,6]. Solvent bonding poses as a low-cost, rapid approach that allows for good optical transparency and robust bonding strength, especially when integrated with thermal bonding. Its challenges include the necessity of use of pre-functionalized channels, channel deformation, and issues rising with solvent residues [25,26]. Thermal fusion bonding is another fast method that produces strong bonding, but it is limited via potential channel deformations, as well as restrictions in the minimization of channel dimensions [27,28]. Chemical bonding is a method that enables strong bonds employing the use of covalent bonding, while it can provide a pathway to simultaneously functionalize surfaces (as for example biomolecule immobilization, or control of wettability) it is considered as a complex and time-consuming process with commercialization limitations [11]. Laser welding is another rapid method that allows for pre-functionalization, and offers high bonding strength. However, it necessitates strict requirements for its use, i.e. simultaneously transparent and absorbent layer, high clamping pressure, and good surface finish. It is known that it also induces thermal stresses throughout the polymer, which can lead to deformations on the microfluidic chip [30,31]. Ultrasonic welding is ultra-fast and inexpensive as a technology, and is suitable for use in mass production, has high bonding strength, and allows for pre-functionalizing channels prior to bonding. Unfortunately for the field, it has been proven that its use occasionally leads to channel deformation, clogging, formation of gaps between bonded layers, and that it constraints channel heights due to the self-induced polymer shrinkage of the method [32,33]. Lei et al. introduced a microwave-based bonding technology, in which thin-film metal (gold) was pre-deposited on the microfluidic chip interface using an electron beam process [34]. Although this method achieved the bonding of PMMA chips at 10 W within 120 seconds, the selective nature of microwaves, which is limited to materials that are relatively transparent to microwaves, as well as the necessity of depositing metal films, render this approach less suitable for low-cost, rapid manufacturing. Another study, achieved efficient bonding in polymer-microfluidic devices by applying a 300 W high-frequency electromagnetic field and microwave energy to polyaniline (a conductive polymer) [35,36]. However, the high energy consumption and specialized equipment requirements appear to limit the broader application of this technology. Additionally, there are more advanced and modern methods that are introduced recently, as for example gas-assisted thermal bonding, which shows potential for the creation of reliable microfluidic devices with thermoplastics. The biggest hurdle for using these sophisticated and advanced new bonding technology it that they necessitate and require the development of specialized, complex equipment that are not currently used in industry [37].

Thermoplastic polymers are some of the most important materials in microfluidics, however, due to the diverse methods and requirements for bonding, thermoplastic adhesion always poses as a significant challenge [38–40]. Researchers have highlighted this complexity and the necessity for introducing innovative solutions in numerous works [18,21,41]. Given this mixed situation with advantages and challenges, there is a paramount need to invent and propose a method that combines the strengths of existing ones, while simultaneously manages to mitigate their limitations. In an effort to find the optimum bonding methodology, Matteucci et al. compared ultrasonic welding and thermal bonding for integrating thin film metal electrodes in injection molded microfluidic chips, showcasing that the former bonded chips showed significantly superior performance [42]. The research employed ultrasonic welding and thermal bonding technology, where the thin-film metal electrodes functioned solely as sensors for analytical purposes. These electrodes served as bonded objects but did not actively participate in the bonding process, not taking advantage of their presence in the chip.

However, despite the research community's efforts to investigate ways that can extend and develop further the traditional bonding technologies, breakthroughs and novel methods that can become a paradigm for bonding have been scarce in literature. Evidently, it is necessary to develop novel processes that can combine the need to be straightforward in their implementation, cost-effectiveness, as well as flexibility and adaptability to different materials and chip designs, avoiding the use of exotic equipment that would dramatically increase their cost-effectiveness.

The current paper, aims to address the above-mentioned challenge of bonding methods for microfluidic chips and to provide a new sustainable pathway, which can become a new paradigm in the field. Herein, the researchers propose and develop a novel thermoplastic microfluidic chip bonding technology that is based on microelectrode heating. This new method addresses the demands for sustainability, i.e. reliability, low cost, and high throughput without the need of use of exotic or dangerous materials. Aiming to achieve the rapid bonding of chosen microfluidic chips, a small-batch customization and electrodeposition of nickel microelectrodes is applied on top of PMMA microfluidic chips. These chips are fabricated using microinjection molding. This proposed method is very simple, as it does not require expensive or complex equipment, while it shows potential for eradicating numerous limitations of other methods, positively influencing the final manufacturing cost. The ultimate goal is to uphold high bonding strength and minimal microchannel deformation. The researchers use a series of characterization methodologies to validate the proposed bonding process and explore its applications, having in mind further developments that can be underpinned with this for all microfluidic technology and its applications.

2 Materials and Methods

2.1 Materials

Poly (methyl methacrylate) (PMMA), is a low-cost polymer material that is commonly used in microfluidic chips. The main material used in this work is a commercial PMMA (CM 205, Chi Mei, Taiwan) whose properties are well known in literature [43]. Nickel (Ni, VALE INCO, Canada) shows excellent thermal and electrical conductivity, mechanical strength, thermal stability, compatibility with electrodeposition, and biocompatibility [44]. These properties make it an ideal material for achieving uniform heating, precise bonding control, and consistent bonding quality in microfluidic chip fabrication. Mechanical strength allows it to maintain stable shape and functionality in microstructures, while its thermal stability ensures that it does not deform or suffer performance degradation during bonding. As a non-precious metal, nickel is abundant, offering both economic and sustainable benefits.

2.2 Microelectrode bonding process

The bonding process based on microelectrodes for microfluidic chips and is used in this work is depicted in Fig. 1 (a). This process is called microelectrode bonding technology (MB) and can be described as follows. Initially, the patterned microelectrodes are placed onto the substrate in designated positions. Subsequently, a cover sheet is placed over the chip and the microelectrodes, followed by pressure and voltage that are applied to the assembled chip. At this juncture, the microfluidic chip gradually joins together, due to the heat that is generated by the microelectrodes and the pressure applied. The core working principle is that when current passes through microelectrodes, the resistance generates heat according to Joule's law, subsequently causing the microelectrodes to increase their temperature and generate bonding energy. This temperature increase is controlled by adjusting the current's magnitude and the duration of its application. This heat allows for the surface locally to exceed the glass transition temperature (T_g) even up to the melting temperature (T_m) of the polymer, and in combination with pressure, it allows for the fusion of the substrates. Additionally, the maximum temperature of the microelectrodes can be controlled by adjusting the applied voltage or duration. When the microelectrode temperature is maintained between the T_g and T_m, the microchannels are primarily sealed through molecular chain diffusion or entanglement [27]. At this stage, this process can be termed microelectrode bonding. However, microelectrode bonding requires prolonged bonding time. When the microelectrode temperature exceeds the T_m, the chip undergoes fusion welding. In summary, the bonding mechanism and strength, controlled according to the application, are also distinctive attributes of this process. Finally, by unloading the bonding voltage, cooling the chip back to room temperature, and removing the pressure, the microelectrode bonding process is complete. The main equipment employed uses a power supply and a small bench vice. This bench vice is primarily used to apply pressure, which is controlled via a torque wrench. The parameters for the bonding experiment are shown in Table 1.

Table 1: The microelectrode bonding parameters.

No.	Voltage (V)	Pressure (kPa)	Time (s)
1	2.5	60	5
2	2.7	90	10
3	2.9	120	15

To clearly understand how well the microelectrode bonding performance is achieved, an adhesive technology is set as the control. The bonding medium is a polyethylene terephthalate film (PET), which is similar to a double-sided tape (Darit tape, China), with a thickness of 0.01 mm.

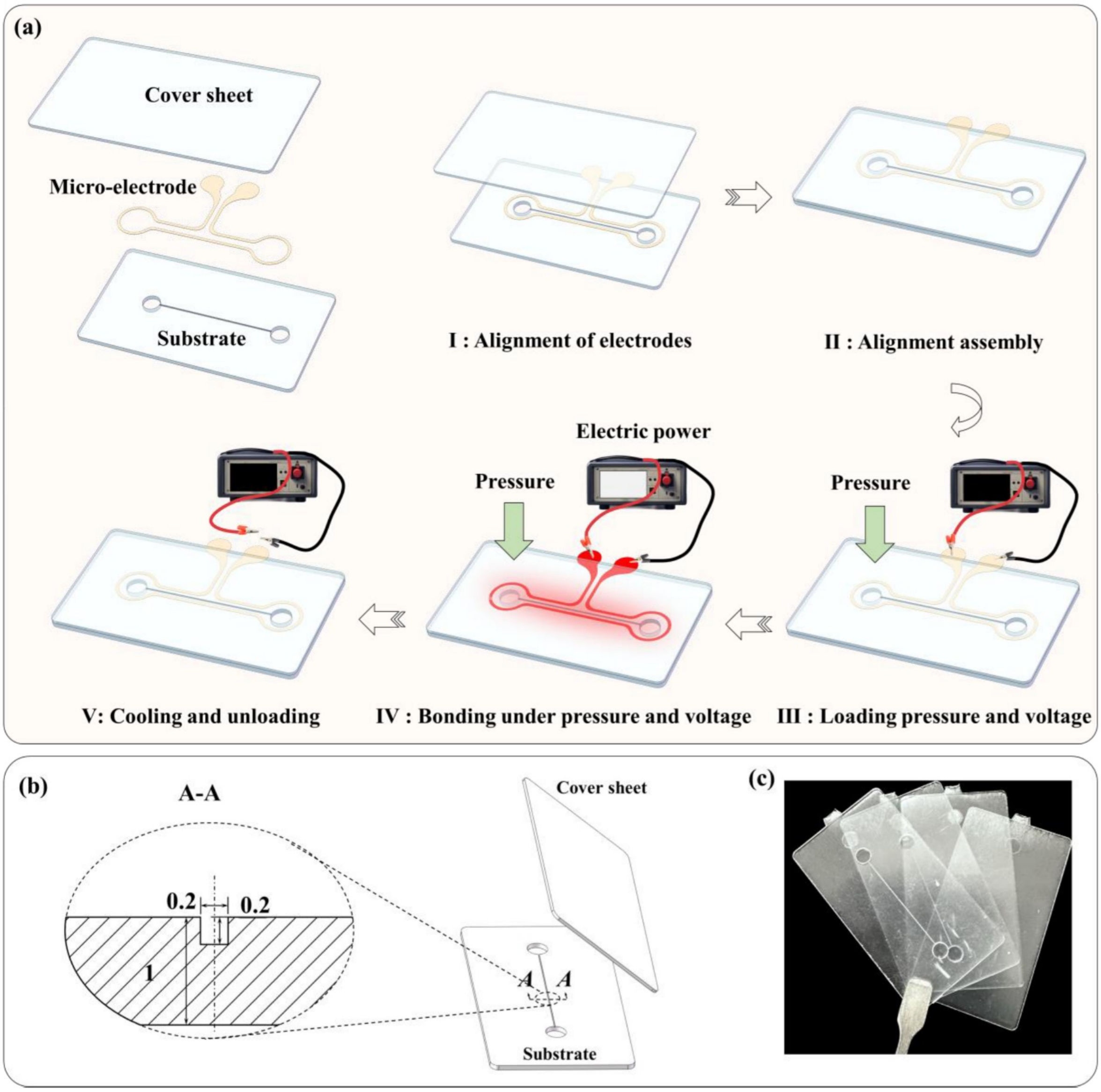

Figure 1: (a) The process flow diagram of the proposed microelectrode bonding process. I: The microelectrode is placed onto the substrate. II: The cover sheet is placed over the chip and the microelectrode. III: Pressure and voltage are applied to the assembled chip. IV: The microfluidic chip gradually reaches temperature over T_m and bonds together under the heat that is generated by the microelectrodes and the pressure. V: Cooling of the chip back to room temperature via unloading the bonding voltage, and removing the pressure, to complete the microelectrode bonding process. (b) Schematic representation of the single-channel microfluidic chip's structure and parameters. The microchannel cross-section is a 0.2×0.2 mm rectangle. (c) Typical single-channel microfluidic chip that is fabricated by microinjection molding.

2.3 Microfluidic chip

The aim of this work is to validate and introduce a novel microfluidic chip bonding process; hence, a single-channel microfluidic chip is employed to conduct chip bonding experiments based on microelectrodes. The chip is fabricated through injection molding, with its structure and parameters illustrated in detail in Fig. 1 (b and c). The precision injection molding machine (Arburg 370S, Germany) is utilized to produce the single-channel microfluidic chips for bonding. The adopted injection molding parameters are derived from the referenced literature [27,43].

2.4 Electrodeposition

During the bonding process, conformal microelectrodes are used, as illustrated in Fig. 2 (a). First, the microelectrodes are designed based on the microchannels/microstructures of the chip. Their defining structural feature is that the distance between the microelectrodes, as well as both the microchannels and their characteristic structures remain constant. The principle followed is to maintain a constant distance between the microelectrode and the microchannel. The design parameters are microelectrode width, height, and distance from the microchannel. Due to the designed microelectrode dimensions and material characteristics, electrodeposition is employed for the fabrication of the conformal microelectrodes [45–47]. Second, a CO_2 laser is used to engrave PET film as a mask [48–50]. Laser positioning, power and linear speed are critical for precise control of microelectrode manufacturing accuracy. Third, the PET film is glued to a prototype stainless-steel plate. Fourth, insulating the stainless-steel plate. Only the designed microelectrode shape is left exposed. Fifth, connecting the circuit to electrodeposit the microelectrodes. The current density as well as the energization time are also critical for precise microelectrode manufacturing. Sixth, cleaning the cathode and removing the PET mask. At last, finishing the preparation of the microelectrode, via stripping the cathode.

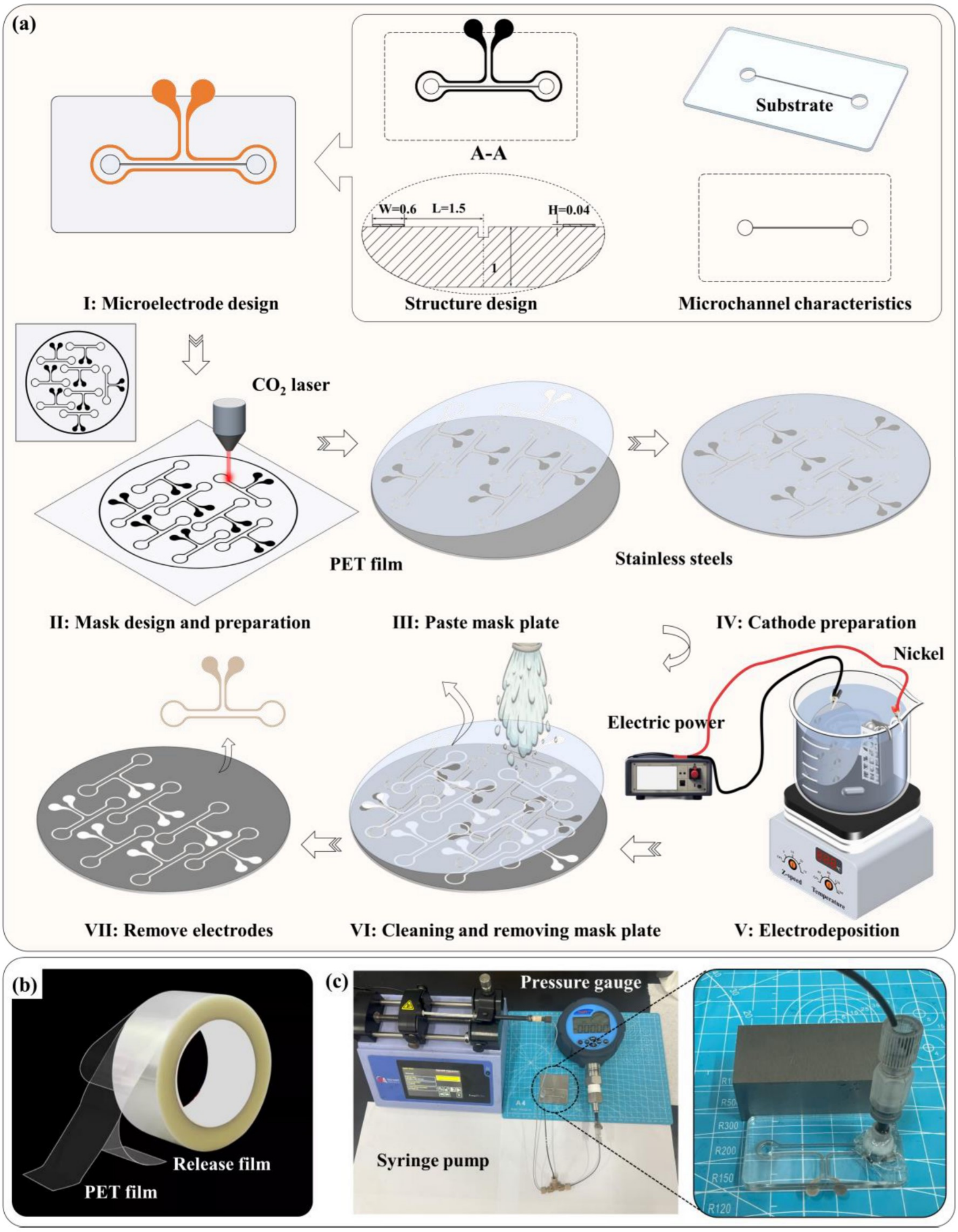

Figure 2: Schematic diagram of the microelectrode fabrication with an electrodeposition process. (a) I: Microelectrodes design according to the microchannel/microstructure of the chip. The principle followed is to maintain a constant distance between the microelectrode and the microchannel. The design parameters are microelectrode width, height, and distance from the microchannel. II: CO_2 laser engraving PET film as

a mask. III: PET film is glued to a prototype stainless steel plate. IV: Insulating the stainless-steel plate. Only the designed microelectrode shape is left exposed. V: Connecting the circuit to electrodeposit the microelectrodes. VI: Cleaning the cathode and removing the PET mask. VII: Finishing the preparation of the microelectrode, via stripping the cathode. (b) The PET film for laser engraving also includes a release film on both sides. (c) Burst pressure test systems include a syringe pump, a pressure gauge, a syringe, and connecting pipes. The microfluidic chip is connected to the pipe by adhesive.

During electrodeposition, the anode can generate impurities. To prevent these impurities from entering the electrodeposition solution, an anode bag (containing nickel beads washed with deionized water) is placed in the anode fixture. A laser engraved mask (high-adhesion PET film) is adhered to the front side of the stainless-steel cathode plate, while its back and surrounding edges are sealed with waterproof insulating tape (PVC, Wapodeai 3PCS Electrical Tape). The microelectrode electrodeposition is carried out using a home-made apparatus (see SFig. 5 in Supplementary Materials). In this setup, the circuit connections are encapsulated, but the power supply and cathode plate are connected via alligator clips, as it can be seen in step V of Fig. 2(a). After electrodeposition completion, the cathode and fixture are separated and rinsed together in deionized water, followed by drying the electroplated layer's surface with nitrogen. The main components of the electrolyte and the basic conditions for the electrodeposition experiments are listed in Table 2.

Table 2. The major ingredients of electrolyte and the working condition.

Ingredient of electrolyte ($g\cdot l^{-1}$)				**Working condition**		
Nickel sulphamidate	**Nickel chloride**	**Boric acid**	**Ethylhexyl sulfate**	**Temperature (°C)**	**Current density ($A\cdot dm^{-2}$)**	**pH**
400	10	30	10	40	0.1, 0.2	3.5–4.5

For the electrodeposition experiments, the anode material is nickel of 99.99% purity (VALE INCO, Canada). Before use, the nickel beads are cleaned with deionized water and ethanol, then dried with a nitrogen gun. The electrodeposition cathode is a 304 stainless steel plate with a diameter of 101.6 mm and a thickness of 2 mm, covered with a conformal microelectrode mask, which is prepared by a CO_2 laser engraving machine (YoungLaser V12, Young Chip, China). The mask is a tape of material 0.5 mm thick (polyester film, PET) and serves solely to expose the conformal microelectrode shapes to the electrodeposition solution and electric field, while covering other non-conductive parts of the cathode (see Fig. 2 (b)). The stainless-steel substrate undergoes degreasing and deionization cleaning prior to electrodeposition. The microelectrode electrodeposition experimental conditions are as follows. The electrode gap is 10 cm, the current density is 4 A/dm^2, and the deposition time is 45 minutes. The power supply equipment used is Agilent B2901A, from Keysight, USA.

2.5 Microelectrode and microchannel morphology characterization

For the quantitative characterization of microelectrodes, an Extended Depth of Field Microscopy (KEYENCE®, VHX-5000, Japan) is used as it is capable of capturing clear images across various different depth ranges. By characterizing and comparing the morphology of microchannels before and after bonding, a deeper understanding of the microelectrode bonding process is achieved, promoting its rational application. The deformation of microchannels is assessed by calculating their cross-sectional area. The methodology for this calculation is as described in Equation 1.

$$\partial = 1 - \frac{\Delta S_a}{\Delta S_b} \tag{1}$$

where ΔS_a is the cross-sectional area of the microchannel after bonding, ΔS_b is the cross-sectional area of the microchannel before bonding.

2.6 Bonding strength characterization

The burst pressure of sealed microchannels is used to characterize the bonding strength [51]. The bonding strength is precisely measured by monitoring the sudden rupture of the sample under pressure, allowing for direct evaluation of the microfluidic chip bonding performance. This method is selected for its direct reflection of the seal's integrity and quality. The detailed testing apparatus and components are shown in Fig. 2(c), and are primarily comprising of a syringe pump (HARVARD APPARATUS®, HA1100D, USA, flow rate range: 1.28 pl/min - 88 ml/min, liner force: 24 kg, accuracy: 0.5%), a precision pressure gauge with data recording capabilities (ConST211, China, range: 0 - 4 MPa, accuracy: 0.05 - 0.2% full range), and a connecting tube. The bonding strength of the microfluidic chip can be directly read from the pressure gauge. Prior to testing, the adapter must be glued to the cleaned microfluidic chip using epoxy resin adhesive and left to set for 6 hours.

2.7 Infrared Imaging

A high-speed infrared camera (ImageIR 8355, InfraTec, Germany) is utilized primarily for observing the uniformity of microelectrode heating and assessing the feasibility of microelectrode application during the microfluidic chip bonding. It is well established that infrared thermal imaging technology plays a crucial role in inspecting heating elements. Therefore, an infrared camera is employed to capture infrared radiation from the surface of microelectrodes and convert it into visualized images of temperature distribution. This approach renders the temperature measurement and monitoring intuitive and contactless.

3 Results and Discussion

3.1 Influence of microelectrode dimensions and process on bonding

This work proposes a microelectrode bonding technology, which employs the bonding principles and mechanisms that are illustrated in Fig. 3(a). Steps i to iii correspond to the microelectrode bonding process (see Fig. 1(a)). Before performing the microelectrode fabrication and bonding experiments, it is crucial to optimally design the microelectrode dimensions (width, W; height, H), placement distance (L), and process parameters (bonding voltage, time, and pressure) to optimize bonding quality and process stability (see Figs. 2(a) and 3(a)). Initially, the electrodeposited patterned microelectrodes are not attached to any flexible substrates (e.g., tape or thin film). Therefore, the designed electrodes must possess sufficient mechanical strength to avoid damage (deformation, bending, fracture) during handling or transfer. Microelectrodes that are too narrow or thin increase these risks. However, significant increase to the electrode size is not feasible, as larger dimensions lead to higher resistance, which subsequently increases the bonding energy consumption. While an increase in the width enhances the bonding area and the contact surface of the microchannel, thus improving bonding strength, an increase in height may result in incomplete microchannel sealing. Thus, one of the design principles for microelectrode dimensions is to appropriately increase the width-to-height ratio, while keeping the height at a minimum level to ensure sufficient mechanical strength. Additionally, one advantage of pure electrodes is that they avoid introducing other flexible materials, which could affect microfluidic analysis, such as introducing toxic substances or causing microchannel blockages.

Furthermore, the optimization of microelectrode dimensions and the selection of bonding parameters can be precisely determined using finite element analysis simulations. For instance, the impact of in-plane microelectrode morphology on current density and Joule heating is illustrated in SFig. 3 and SFig. 4. The results of this study indicate that the design principle for in-plane microelectrodes is to avoid sharp or right angles in electrodes that are placed on both sides of the microchannel, in order to prevent thermal stress concentration. (For details on the finite element simulation model, material properties, and boundary conditions established based on a 1:1 scale of the chip, see SFigs. 1-4.) The temperature variation of the microelectrode, under different voltage conditions over time is shown in Fig. 3(b). The results prove that under different bonding voltages, the microelectrode reaches and stabilizes at different peak temperatures, rather than a continuous increase over time. The reason is that there is a significant heat exchange taking place between the microelectrode, the microfluidic chip, and the bonding equipment. Evidently, the heat generated and dissipated by the microelectrode reaches an equilibrium. To verify this conclusion, simulations are performed to consider the temperature rise of the microelectrode under both heat transfer and thermal insulation conditions, as shown in Fig. 3(c). The results show that with a bonding voltage of 2.65 V, the microelectrode reaches and stabilizes at a peak temperature of 263.56°C after 11 s. Without considering heat transfer (thermal insulation), the microelectrode reaches 593.84°C after 15 s. This showcases that, during microelectrode bonding, the addition of thermal insulation pads can concentrate heat more effectively around the microelectrode, and improve process stability, while avoiding microchannel deformation caused by excessive temperatures. In parallel, one can understand that the phenomenon of peak temperature at different voltages is critical for the stability of the proposed microelectrode bonding process. This indicates that when the uniformity of microelectrode dimensions is adequately supported by mass production technologies, microelectrodes will be able to stably bond microfluidic chips at a fixed bonding voltage. Therefore, the precise control of microelectrode bonding temperature through the control of bonding voltage is one of the advantages of this technology. Subsequently, it is proven that the microelectrode bonding process exhibits stable characteristics, with the stability of bonding quality depending primarily on the fabrication precision of the microelectrode dimensions.

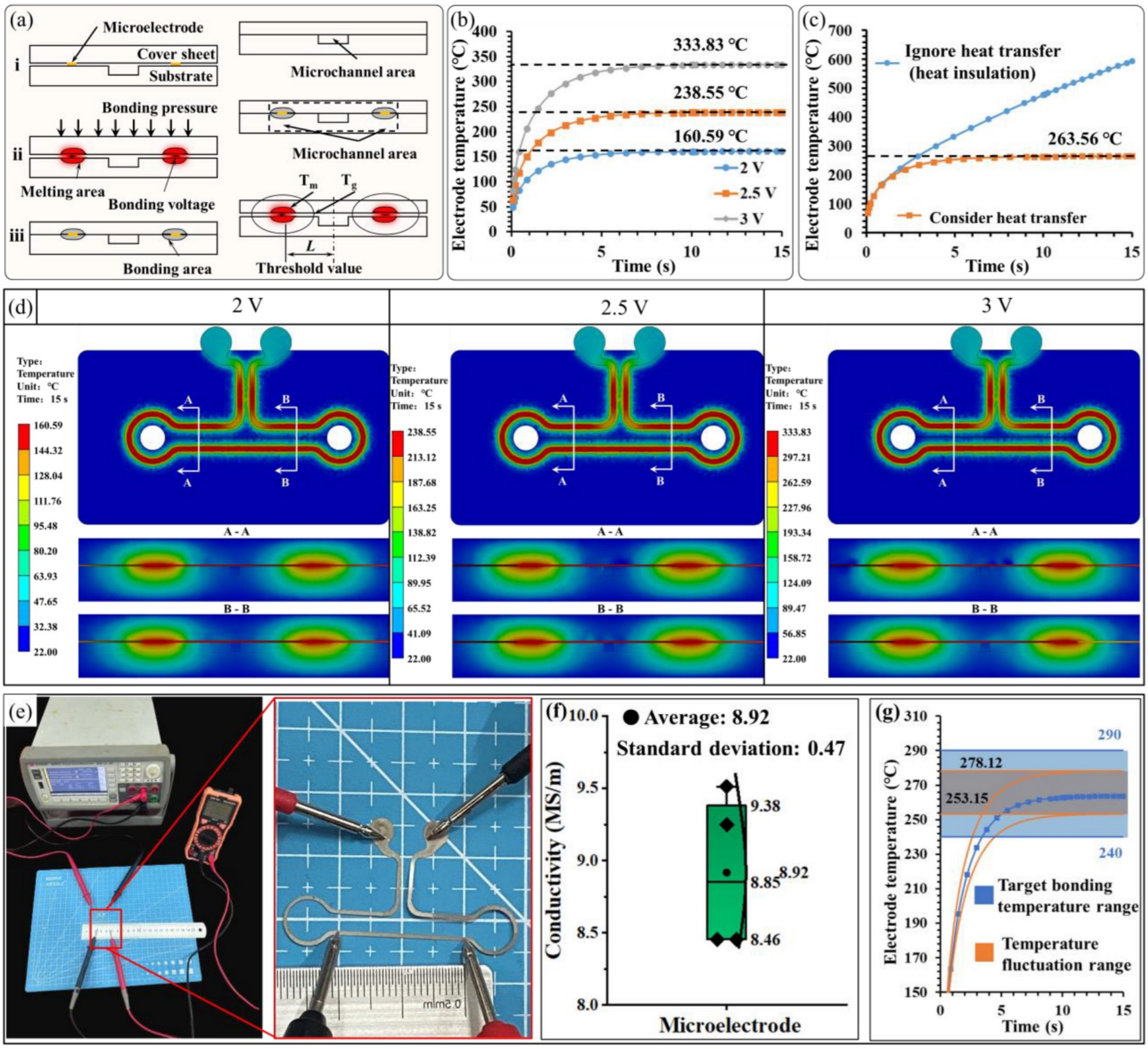

Figure 3. (a) Schematic diagram of the microelectrode bonding mechanism. (b) Graph showing the temperature variation of the microelectrode, under different voltage conditions over time. (c) Graph showing the temperature rises of the microelectrode, under both heat transfer, and thermal insulation conditions. (d) The distribution of temperature curves near the microelectrode and the microchannel under different bonding voltages. (e) The four-point probe method used to accurately measure the electrical conductivity of the samples. (f) The electrical conductivity of the four microelectrodes and its distribution. The fluctuation range of the conductivity is less than 5.29% of the mean value. (g) Graph showing the electron temperature versus time. Notice that the range of maximum temperature variation in the microelectrodes caused by conductivity fluctuations remains within the ideal bonding temperature range.

After determining the basic dimensions of the microelectrode, the bonding parameters are set based on two factors. Bonding voltage, which is determined by the temperature at which the microelectrode reaches its peak, and the bonding time, which is determined by the time period required for the microelectrode temperature to stabilize. The microelectrode temperature is set according to the melting temperature of the microfluidic chip material. In this case, the injection molding temperature range for PMMA is 240 - 290°C, therefore the optimal bonding temperature is selected within this range. Temperatures below this range result in incomplete bonding and low bonding strength, while exceeding this range leads to polymer thermal decomposition and significant deformation or blockage of the microchannel. Bonding time appears to invoke similar effects. A bonding time that is too short prevents the microelectrode from reaching its peak temperature, reducing bonding strength and process stability, while excessive bonding time decreases bonding efficiency.

The appropriate design of the distance between the microelectrode and the microchannel is essential for the precise control of the microchannel height. When this distance is below the threshold, even a low bonding pressure can cause significant microchannel deformation due to excessively high temperatures around the microchannel. Only when the microelectrode position exceeds the threshold will the impact of bonding temperature be minimized. Thus, the design principle for the microelectrode position threshold is that when the microelectrode temperature reaches or exceeds the polymer's melting temperature, the temperature near the microchannel must remain below its glass transition temperature to avoid significant deformation. The definition of this threshold can be found in Fig. 3(a). Fig. 3(d) displays the distribution of temperature curves near the microelectrode and microchannel under different bonding voltages, which serves as an important reference for the determination of the microchannel placement distance. Accordingly, hugely increasing the microelectrode placement distance enlarges the in-plane microchannel area (see Fig. 3(a)), and, thereby, the size of the microfluidic chip. This threshold is also influenced by parameters such as microelectrode material (resistance, conductivity), cross-sectional area, length, and bonding voltage. Therefore, conducting finite element simulations during the microelectrode bonding design phase is necessary to optimize these parameters.

The electrical conductivity of the electrodeposited nickel electrodes also plays a crucial role in determining the efficiency and uniformity of the Joule heating process. In this work, the electrical conductivity of the nickel electrodes is measured to ensure consistency, and to evaluate the potential impact on scaling up the bonding process. The four-point probe method is employed to accurately determine the electrical conductivity (σ) of the sample. This method, known for minimizing contact resistance effects, is adapted to account for the microelectrodes. The power supply described in Section 2.4 is used to provide a stable 1 A direct current (I) for the experiments. The four probes are arranged as shown in Fig. 3(e). A known current is applied through the two outer probes, and the voltage drop (V) is measured across the two inner probes. The distance between the electrodes is denoted as L. The electrical conductivity is calculated using the equation $\sigma=(L\cdot \mathrm{I})/(\mathrm{V}\cdot \mathrm{A})$, where A is the cross-sectional area of the microelectrodes. The conductivity measurements performed for the four microelectrodes are shown in Fig. 3(f), having a fluctuation range of 5.29%. Based on this fluctuation range, follow up simulations assess the effect of electrical conductivity on the maximum temperature of the microelectrodes under identical process conditions, as illustrated in Fig. 3(g). The temperature fluctuation range caused by variations in electrical conductivity is found to be 253 - 278°C, which is within the ideal bonding temperature range (240 - 290°C). One can see that while the microelectrode bonding process allows for precise temperature control, the bonding stability is dependent on the consistency of the microelectrode fabrication process and the stability of its electrical conductivity. The study results demonstrate that the fluctuation in the maximum heating temperature, caused by differences in the electrical conductivity of electrodeposited microelectrodes, remains within the ideal bonding temperature range. This finding establishes a theoretical foundation for achieving efficient and stable microelectrode bonding and provides a crucial basis for optimizing their performance.

The bonding pressure is the last factor to be considered. Based on the schematic of the microelectrode bonding process (see Fig. 3(a)) and the stability analysis of microelectrode temperature, once the microelectrode temperature and position are determined, the only process parameter affecting the microchannel height is the bonding pressure. Therefore, when the polymer surrounding the microelectrode reaches its melting temperature, applying an appropriate bonding pressure is sufficient to seal the microchannel. Increased bonding pressure is the direct cause of microchannel deformation. Thus, precisely controlling the bonding pressure uniformly and keeping it as low as possible during microchannel sealing is crucial for accurately controlling the microchannel height. Additionally, compared to thermal bonding and ultrasonic welding, the lower bonding pressure (by 1-2 orders of magnitude) is a distinct advantage of microelectrode bonding technology.

3.2 Microelectrode morphology and heating

The physical form and surface characteristics of microelectrodes significantly impact their performance, particularly in heat generation and conduction for applications such as polymer melting during the microfluidic chip bonding processes. Fig. 4(a) shows the PET mask, cathode, and electrodeposited microelectrode, respectively. The mask plate is quickly and easily prepared (40 s) with the laser engraving equipment, aided by computer assisted design, to enable rapid iteration of the microelectrode structure. Subsequently, the microelectrodes are separated intact from the stainless-steel cathode. This demonstrates that the electrodeposition process can be adapted to microelectrode processing. It is important to note that the precision in microelectrode manufacturing determines their dimensional accuracy, which in turn influences their heating uniformity. The latter is an essential factor for the reliable microfluidic device operation. Consequently, Fig. 4(b) elucidates the morphology of microelectrodes prepared by electrodeposition. The results indicate a deviation between the microelectrodes that are prepared by laser-engraved masking followed by electrodeposition and their designed dimensions. The cross-sectional profile of the microelectrodes, averaged over 20 profile lines, appears as a trapezoid as depicted in Fig. 4(d), with base, top, and height dimensions of 649.69 μm, 592.25 μm, and 37.49 μm respectively. The deviation springs from the enlargement of dimensions that are caused by the laser heat, which is scorching during the mask engraving process. This error is typically eliminated by adjusting the laser intensity or the design dimensions. Similarly, thickness deviation is rectified by modifying the electrodeposition duration. However, when used as heating elements, the surface flatness and uniformity of the microelectrodes are of paramount importance. This is due to the fact that only microelectrodes with consistent physical characteristics ensure uniform heating effects. Any sudden changes in local dimensions result in rapid or slow temperature changes, causing uneven bonding, which typically manifests as scorching or leaks in the final fabricated microfluidic chips. Despite dimensional inaccuracies and micro-pits on the surface, the overall shape of the microelectrode is regular and intact. Consequently, these electrodes are appropriate to be used for microfluidic chip bonding. Evidently, electrodeposition is affirmed as an ideal process for preparing this type of microelectrodes.

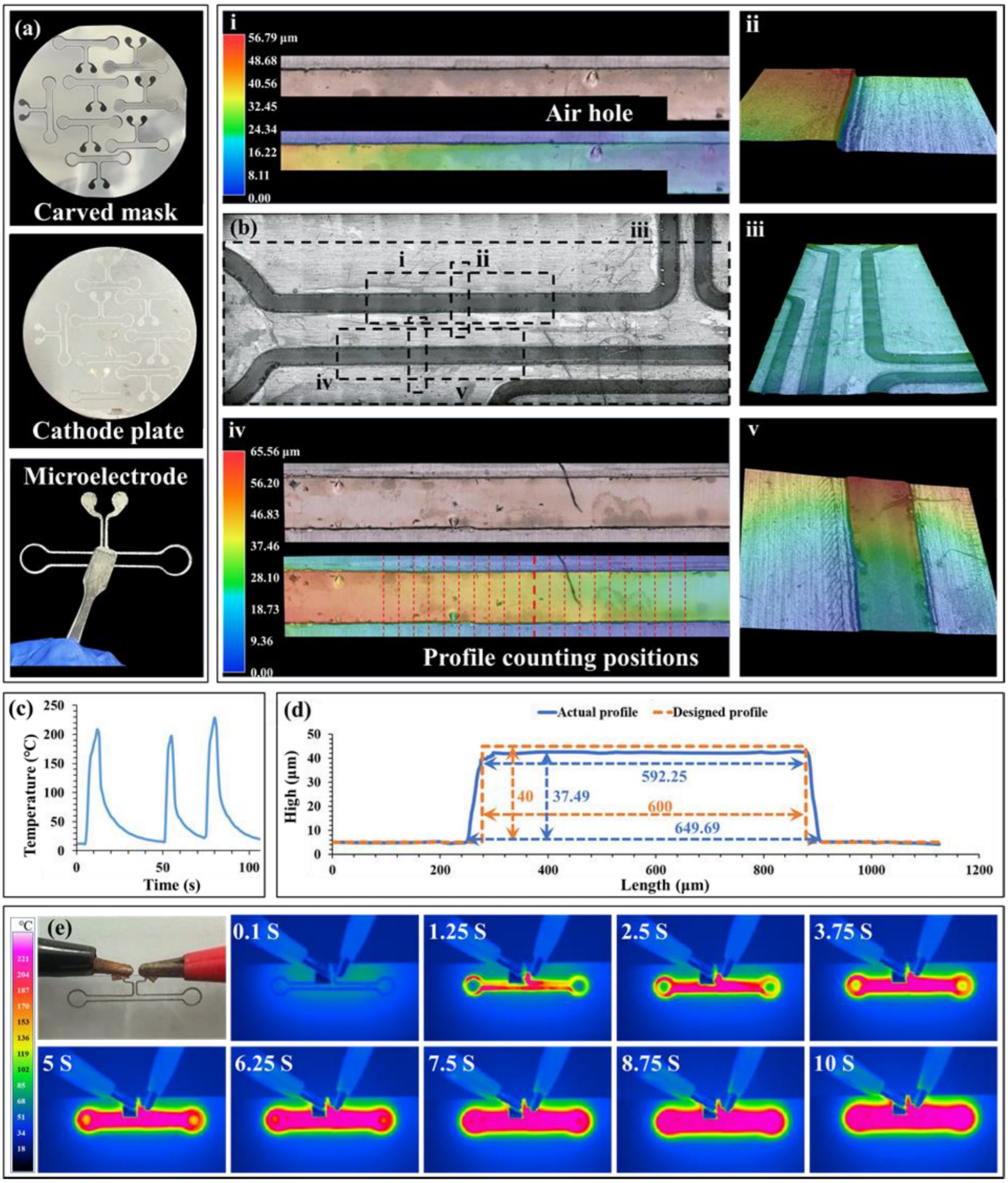

Figure 4: The structure, morphology and heating properties of electrodeposited microelectrodes. (a) The PET mask, cathode, and electrodeposited microelectrode. (b) The surface morphology of electrodeposited microelectrode. (i-v) The 3D morphology of different regional locations. Notice that the overall uniform structure is able to meet the bonding requirements, with the exception of a few holes. (c) Temperature profile of multiple heating of the microelectrode in air at bonding voltage of 3V. (d) Differences between

microelectrode profiles (averaged from 20 profiles, positions referenced to (b) (iv)) and design profiles. It is important to note that machining errors are within acceptable limits. (e) Microelectrode heating uniformity is characterized by infrared thermography at a 3V bonding voltage. Notice that after 4 seconds, there is a uniform microelectrode heat distribution.

The heating rate is the initial focus in the discussion of the microelectrode heating performance. The material for this specific microelectrode is nickel, an excellent thermal conductor, which efficiently converts electrical energy into heat. The heating rate of the microelectrode, as well as the temperature rise curve at ambient temperature with an applied voltage of 3 V, are depicted in Fig. 4(c). The test results showcase a heating rate that ranges between 40-80 °C/s, showcasing that it allows for PMMA to achieve the T_m rapidly. As documented in literature [27], T_m of PMMA CM-205 is about 240°C. This rapid heating renders microelectrode bonding technology advantageous comparing to others in literature, as it enables rapid high-strength thermal fusion in solely a few seconds. Theoretically, the microfluidic chips can be heated to the molten state within approximately 3-6 seconds. However, further increasing the heating rate may lead to issues such as polymer volatilization. Extending the bonding time marginally helps optimize these issues based on the observed heat transfer between the chip and the pressure apparatus during pressure application. To elucidate the mechanism and calculate the real required voltage and time, one must determine them through additional experiments.

Fig. 4(e) shows a series of infrared thermal images that are depicting the heating of microelectrodes. Due to their 40 μm thickness, the microelectrodes are prone to warping and deformation in air. As previously mentioned, this is caused by the rapid heating and stress concentration during the heating process. To circumvent this issue, the microelectrodes must be clamped between two glass slides. However, infrared is absorbed or reflected when passing through glass, which means that infrared images taken through glass may not accurately depict the reality. This approach is appropriate as the aim is to analyze the microelectrode heating uniformity, and the precise temperature rise curve of the microelectrode is already demonstrated in Fig. 4(c). It needs to be clarified that, therefore, the provided temperature scale in Fig. 4(e) is for reference. Nonetheless, the images reveal that heat is primarily concentrated in the areas where the electrodes connect. In terms of heat distribution uniformity, infrared imaging in the first 3 seconds clearly shows variations, with the central part of the electrode heating faster than its ends. Over time, the heat disperses across the entire electrode, achieving a relatively uniform distribution after 4 seconds of power application. This is attributed to geometric factors (uniform contact (guaranteed by bonding pressure), and electrode size) affecting heat conduction. Following this characterization, the researchers suggest that for microfluidic chip bonding applications, the voltage should be lowered and the duration extended. Regarding, other applications that might require a more detailed and in depth understanding of the thermodynamics, as well as the ones that have less margin of tolerance, further experimental analysis is required in order to achieve more precise and controlled microfluidic chip bonding.

3.3 Bonding performance

This section presents the microelectrode bonding experiments conducted on the microfluidic chip. The microelectrode-based microfluidic chip bonding process is simple and only uses a power supply and a small vise (see Fig 5(a)). The results demonstrate that when a 3 V voltage and a 10 s bonding time are applied, one can observe significant bonding traces around the microelectrodes. The microelectrodes, upon heating, allowed the surrounding areas of the microfluidic chip to have temperatures over the T_m, leaving behind bonding traces as can be seen in Fig. 5(a). This clearly evidences the feasibility of the microelectrode bonding process. The bonding traces that appear on both sides of the microelectrodes showcase that the microfluidic chip is heated to the molten state, and is subsequently merging the cover sheet and the substrate together. Simultaneously, a certain distance between the named bonding traces and the microchannels still remains. This suggests that the molten polymer does not flow through, and does not result in the blocking of the microchannels. Therefore, as long as the distance between the microelectrodes and the microstructures is controlled, it effectively mitigates or avoids completely any creation of the microstructure deformations.

Considering the optimization of the proposed bonding process (as well as any other bonding process), it needs to be in alignment with applications, whereas the bonding strength of the microfluidic chip and the morphology of the microchannels are comprehensively considered. Results from bonding experiments reveal that when the voltage is below 2.5 V, the microfluidic chip seal unsuccessfully within the 15 seconds, although bonding traces can still be identified. The primary reason lies in the fact that the microelectrodes are not capable of generating the sufficient amount of heat that is required to reach the T_m of the polymer, with a 2.5 V voltage. Additionally, the significant heat conduction that exists between the chip and the holding vice is also a factor that results in the above-mentioned phenomenon. Several measures are implemented to address these issues. The voltage is increased to 2.7-2.8 V, and there is an implementation and usage of thermal insulation pads to allow for a well-bonded chip (see Fig. 5(b)). In this work, the microelectrode has a thickness of 0.04 mm, which is $1/45^{\text{th}}$ the thickness of the microfluidic chip (1.8 mm). The impact of the microelectrode thickness is negligible, even when it reaches the polymer's melting temperature (see SFig. 6). Uniform heat generation, coupled with the parallel application of bonding pressure, ensures that the microelectrode remains free from warping or deformation. This is further corroborated by the bonding experiments shown in Figs 5(a) and (b), which demonstrate that there is no evidence of deformation. In reality, uniform thermal cycling helps to relieve residual stress in the chip, ultimately improving its flatness. The bonded microchannel successfully facilitates capillary-driven flow of the indicator liquid (shown in Fig. 5(b)). Furthermore, high-resolution microscopy of the reconstructed microchannel morphology (as seen in Fig. 5(g)) appears to have no evidence of channel closure. Fig. 5(c) shows the burst pressure profiles of four samples, when the bonding process parameters are 2.8 V, 60 kPa, and 15 s. The results indicate that when employing the microelectrode bonding technology, the bonding strength of the chip exceeds 2.9 MPa, as the chip did not separate as initially predicted and anticipated at this value. During the testing process, the chip joints that are bonded by epoxy resin adhesive are the first to detach from the chip due to the applied pressure (Fig. 5(d)). This shows clearly and provides evidence that within the testing system, the adhesive-bonded connectors are the weakest points in terms of strength. From this experiment, we can logically claim that the strength achieved with the proposed bonding process is larger than 2.9 MPa.

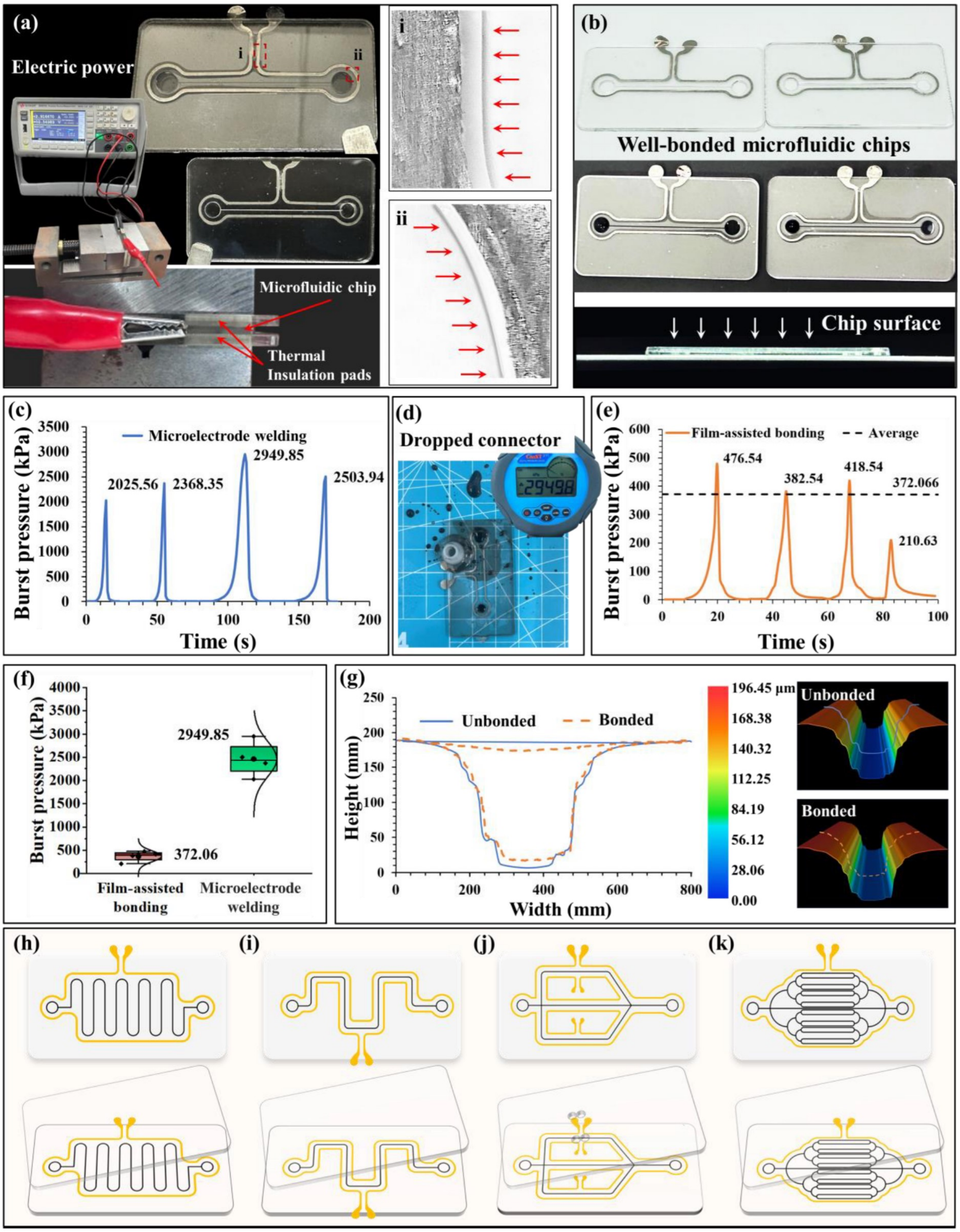

Figure 5: Microelectrode bonding performance of microfluidic chips. (a) The microelectrode bonding apparatus, which requires only an electrical power supply and a small vise. (i-ii) Examples of microscope images that show bonding traces observed at different positions. (b) Photos of the well-bonded microfluidic chips. (c) Graph of burst pressure versus time, showing the burst pressure curve for 4 different chips that bonded at 2.8 V and 60 kPa with 15 s. (d) Photo of the adhesive connector used, as it fails during the burst pressure test, showcasing that the chip's bond strength is greater than 2.9 MPa. (e) Plots of burst pressure versus time for the same four burst pressure curves of the chips that are bonded with PET film. (f) Graph of burst pressure versus time, comparing the microelectrode bonding with film-assisted bonding, where the former exhibits higher burst pressure than the latter. (g) Plots and graphs of microchannel profiles before and after microelectrode bonding. The results show that microelectrode-bonded microchannel deformation is less than 10% comparing to pre-bonding. (h) Schematic of microelectrode bonding schemes that can be adopted for dense serpentine microchannels. (i) Schematic of the high sealing requirements of serpentine microchannels. These can be addressed by increasing the chip bonding area as seen here. (j) Schematic showing the sealing of annular microchannels. This places new demands on the bonding scheme. (k) Schematic representation of dense mesh microchannels, showing that the suitability of microelectrode bonding depends on the application requirements. Microelectrode bonding still shows advantages in most application cases.

For direct comparison, adhesive bonding technology is used to bond the same microfluidic chips. The continuous burst test curves for four samples are plotted in Fig. 5(e). The test results clearly evidence that with increasing test pressure, leakage phenomena consistently occur at the bonding interfaces of the test samples. The average bonding strength of adhesive bonding is 372.06 kPa, which is significantly lower than the microelectrode bonding strength of 2949.85 kPa (see Fig. 5(f)). This provides a considerable advantage in bonding strength for the microelectrode bonding. Regarding the bonding strength formation mechanism, the adhesive bonding or the film-assisted bonding primarily rely on the bonding of molecular chains that provide the necessary bonding strength. Microelectrode bonding on the other hand achieves bonding by using a mechanism of heating the microfluidic chips to T_m, followed by merging and cooling, via integrating the cover and base substrates into one. Theoretically, microelectrode bonding can enhance the bonding strength of the chips to reach the inherent strength of the material itself. In the examined current case, it is indeed proven that the strength derived from microelectrode bonding considerably exceeds the one that is obtained through interlocking molecular chains or chemical bonds.

Microchannel deformation is also a critical process parameter, since it significantly influences both the chip performance, as well as its intended function. The microchannel morphology before and after bonding, along with the microchannel deformation, are depicted in Fig. 5(g). The results reveal a microchannel deformation of 9.9%. The minor deformation is characterized by the depression of the cover piece as well as the decreasing microchannel height. This indicates that the rapidly generated heat is relatively concentrated near the microelectrode without causing a sudden temperature rise in the microchannel. On the other hand, it also shows that the 60 kPa pressure satisfies the bonding requirements without causing significant deformation. According to current literature, the state-of-the art for a microchannel deformation rate is 15% with a bonding strength of 0.64 MPa under the process parameter combination (pressure: 0.35MPa) using thermal bonding technology [27].

To summarize the above findings, the current study has shown that the proposed microelectrode bonding achieves lower microchannel deformation (9.9%) and higher bonding strength (>2.9 MPa), while using lower pressure (0.06 MPa). Additionally, microelectrode bonding does not necessitate the use of complex equipment. One can therefore conclude that the innovative process design of using microelectrodes for microfluidic chip bonding exhibits significant advantages over the traditional bonding methodologies. Finally, it should be emphasized that the microelectrode bonding method, in its current form, is optimized for thermoplastic polymer-based materials (in this case PMMA). The authors expect that direct bonding of non-polymeric materials, as for example silicon, silicon oxides, silicon nitrides, and silicon carbides, is not feasible without severe method modifications.

3.4 Advantages and limitations of microelectrode bonding comparing with literature

The discussion regarding the advantages of microelectrode bonding, revolves around efficiency, performance, cost, equipment complexity, and safety aspects. Table 3 summarizes the literature in bonding performance of microfluidic devices that use thermoplastic materials over the last ten years. Starting with efficiency, in comparison with thermal bonding and solvent bonding, which can take several minutes to tens of minutes, microelectrode bonding demonstrates a clear advantage, with times spanning to the regions of tens of seconds (in this case less than 15s). Other processes include laser and ultrasonic welding. Even when considering the preparation time for microelectrodes, microelectrode bonding technology can still be holding the potential for further efficiency improvements. While ultrasonic welding (UW) is indeed suitable for large-scale manufacturing, the proposed microelectrode bonding offers unique advantages. These are the precise heat control, the lower energy consumption, and the cost-effectiveness in combination with minimal equipment requirements. In MB, the heat is generated through localized Joule heating of the microelectrodes, allowing the precise control of the temperature distribution and the heating duration (detailed in Section 3.1). Contrarily, UW relies on mechanical vibrations to generate heat, which leads to poor control of temperatures, subsequent warping or distortion, especially in the case of smaller microfluidic structures. Moreover, the parameter combination of ultrasonic welding, needs to be obtained through a lot of basic experiments. As evidenced in previous chapters, MB operates at low voltages (2.5-2.9 V) and requires significantly less energy than UW, which needs high-frequency vibrations and substantial power input. Moreover, MB only requires a simple power supply and a bench vice to apply pressure, which is much less complex than UW systems that require high-frequency vibration generators and acoustic tools. Additionally, the presence of the energy-gathering rib structure further increases the processing difficulty, time, and cost for fabricating the chip or mold. These features make microelectrode bonding a promising approach for applications where precision and minimal deformation are essential.

For thermoplastic microfluidic chips with commercial potential, plasma treatment is typically introduced as an auxiliary or pre-treatment step, during thermal compression bonding processes. As emphasized in the introduction, the combination of multiple techniques inevitably adds to the complexity of a bonding process, not only with additional steps, but also introducing expensive and complex (e.g. low-vacuum) equipment. This is precisely the motivation behind proposing the microelectrode bonding process, which aims to enhance bonding performance while simplifying the process and conditions, and reducing the need for specialized equipment. In summary, even though plasma-activated bonding has profound advantages, i.e. such as room-temperature bonding and minimal thermal input, the microelectrode bonding technique offers the distinct innovations, including of precise thermal control, environmental friendliness, high bonding strength, material versatility, and simplified equipment requirements.

Due to the additional microelectrode production steps introduced by MB technology, the method seems limited in mass production. However, a potential expansion of the cathode plate area in combination with an increasing current density, can lead to a significant enhancement of the fabrication efficiency of single electrode. Moreover, batch fabrication technology, as for example screen printing and 3D printing have the clear potential to further increase production efficiency and reduce bonding costs. With these the single electrode production time can go down to a few minutes, allowing for the lowering also of production costs [52–55]. On the other hand, MB technology has further development potential. For instance, integrating MB into molds (similar to in-mold thermal compression bonding) can offset the limitations brought by additional production steps (see SFig. 7). It is important to emphasize that although this work is not yet complete, the authors are confident that it will be a significant direction for future research. This process only requires minor modifications to the molds, thus simplifying the production process of microfluidic chips by eliminating cleaning and drying steps. However, ultrasound, laser systems, or solvent bonding technology are not suitable for in-mold applications due to the constraints of mold size or bonding efficiency. Furthermore, the overall advantages of MB in terms of bonding efficiency, devices, performances, and operational efficiency are sufficient to offset the impact caused by the microelectrode processing steps.

Considering all the above and to the best of the authors' knowledge, the performance of the above described microelectrode bonding method, which shows burst pressures higher than 2.9 MPa and microchannel deformation rates less than 10% is the best recorded so far in the literature of bonding technologies. When it comes to burst pressure, it may vary with the microchannel structure and dimensions, i.e., the bonding strength decreases when using a complex microchannel for testing. However, the microchannels tested in this study are similar in structure and dimensions to those reported in most references. Therefore, the burst pressure of 2.9 MPa, used as comparative data, has objective confidence and reference value. Additionally, it should be noted that the microelectrode bonding does not require complex additional devices. A controllable power supply and a vice are sufficient to complete chip bonding immediately. Simultaneously, unlike laser methods, which require absorptive materials or the addition of absorbers, microelectrode bonding is suitable for bonding using most of the amorphous transparent materials, corresponding to the ability of the method to avoid impact on optical analyses. Similarly, unlike solvent bonding and film-assisted bonding, which require the introduction of volatile solvents (acetone, isopropanol) and interlayers, microelectrode bonding does not introduce any impurities or chemical reagents, ensuring absolute safety. There are no stringent requirements for the raw materials in microelectrode bonding. Theoretically, any conductive material such as platinum, copper, iron, and carbon fiber can be used to fabricate microelectrodes.

Table 3: Differences between microfluidic chip bonding methods for common thermoplastic materials in terms of process, burst strength, and efficiency.

Method	Material	Effective Parameters	Burst pressure	Published Years	Supplementary	Ref.
Plasma treatment + Surface modification	PDMS-PMMA	Bonding time: 40 min.	622 kPa	2022	/	[56]
Solvent-assisted thermal bonding	PMMA-PMMA	Bonding time: 40 min. Bonding temperature: 70°C. Bonding pressure: 10 kPa.	1000 kPa	2022	Multilayer bonding Propan-2-ol, (IPA, poisonous)	[57]
Solvent Vapor-assisted thermal bonding	COC-COC	Bonding time: 16 min. Bonding temperature: 72°C. Bonding pressure: 3993 – 7985 N.	1700 kPa	2022	60 vol% cyclohexane and 40 vol% acetone (poisonous).	[58]
Film-assisted thermal bonding	PMMA-TPE, PMMA-PMMA	Bonding time: 15 min. Bonding temperature: 84℃ (PMMA), 70℃ (TPE). Bonding pressure: 2.4 MPa (PMMA), 1.6 MPa (TPE).	1000 kPa	2021	/	[59]
Intermediate bonding	PDMS-PMMA	Bonding time: 60 min.	436.65 kPa	2019	Sputter-coated silicon dioxide + oxygen plasma	[60]
Film-assisted thermal bonding	PMMA-film-PMMA	Bonding time: 10 min.	Over 2 MPa	2018	Polyethylene terephthalate + UV curing adhesive	[61]
Solvent-assisted thermal bonding	PMMA-PMMA	Bonding time: 20 min. Bonding temperature: 60°C.	655 kPa	2017	/	[62]
Solvent-assisted thermal bonding	PMMA-PMMA	Bonding time: 15 min. Bonding temperature: 68°C.	660 kPa	2016	Isopropyl alcohol (poisonous)	[63]
Adhesive bonding	PMMA-PDMS	Bonding time: ~5 min.	345 kPa	2021	Biocompatible adhesive tape + oxygen plasma treatment	[64]
Solvent bonding	PLA-PMMA	Bonding time: 30 min. UV light. Annealing temperature: 50°C	1.352 MPa	2018	/	[25]
Thermal bonding	PMMA-PMMA	Bonding time: 5 min. Bonding temperature: 103°C. Bonding pressure: 0.3 MPa	600 kPa	2023	Highly dynamic tempered in-mold thermocompression	[27,65]

					bonding	
Thermal bonding	PMMA-PMMA	Bonding time: 5 min. Bonding temperature: 109°C. Bonding pressure: 1.7 MPa	1.77 MPa	2023	Structural design	[43]
Microelectrode bonding	PMMA-PMMA	Bonding time: 15 s. Bonding voltage: 2.8 V. Bonding pressure: 60 kPa.	Over 2.9 MPa	This work		This work

Nonetheless, there are some limitations for the microelectrode bonding. The microelectrode bonding strategy differs depending on the application, particularly for denser serpentine microchannels. When there is no need to consider fluid exchange between channels, the perimeter can be sealed as shown in Fig. 5(h). Conversely, when stringent control of internal pressure and fluid flow rate in the channels is necessary, microchannels may be fully surrounded (see Fig. 5(i)), though this vastly increases the space that is occupied by the microchannel (see Fig. 3). In cases where the surface area of the microfluidic chip is strictly limited, the viability of the microelectrode bonding process will depend on the sealing integrity between the microchannels and the specific application requirements. It is important to note that ultrasonic and laser welding also face similar challenges, as they require a number of considerations of the laser path and energy-gathering ribs, respectively. This showcases that those chips that are suitable for laser or ultrasonic welding are also amenable to microelectrode bonding, which suggests that the advantages of these methods have subsequently become quite limited. There is also the chance that microelectrode bonding may not be applicable to microfluidic chips with dense microchannel networks and strict fluid control requirements (Fig. 5(k)), since it depends on the requirements of specific application. For the case of the serpentine microchannels (see 5(j)), higher demands are placed on microelectrode fabrication precision, as well as the bonding power source, and the microfluidic chip area. One can clearly see that the microelectrode bonding shares similar application scopes with ultrasonic and laser welding. However, for large storage pools or arrayed micro-structures, microelectrode bonding is more advantageous than thermal compression bonding, which causes significant deformation. Finally, possibly the most substantial challenge faced by microelectrode bonding is the rapid increase in microchannel area. Whether the method is suited for chips with dense networked microchannels, needs to be further and carefully examined to clarify the handling of the appropriate fluid control requirements. For most applications of dense microchannel network, we consider the external enclosure method shown in Fig. 5(k) to be feasible.

4 Conclusions and prospects

The development and commercialization of microfluidic chips have been hindered by the limitations of existing bonding technology, which often result in inadequate bond strength and significant deformation. This study introduces a novel microelectrode bonding technology for microfluidic chips, addressing the critical need for reliable, cost-effective, and high-throughput bonding methods in microfluidic technology. Specially, the bonding or sealing mechanism can be controlled by the applied voltage and duration, i.e., the microelectrode bonding technology.

Our electrodeposition method, utilizing a nickel sulphamidate-based electrolyte and CO_2 laser-engraved PET masks, allowed for the rapid production of microelectrodes precise dimensions (base: 649.69 μm, top: 592.25 μm, height: 37.49 μm). These electrodes demonstrated excellent heating performance, achieving rates of 40-80 °C/s at 3V, enabling rapid polymer melting for bonding. Our research demonstrates that the microelectrode bonding process achieves substantial bonding strength with minimal deformation. Specifically, applying a voltage of 2.8V, a pressure of 60 kPa, and time of 15s results in bond strengths exceeding 2.9 MPa. This method marks a substantial improvement over traditional adhesive bonding technology, which exhibit average bond strengths around 372.06 kPa. Additionally, the process ensures minimal deformation due to the rapid and controlled heat generation at the bonding interface.

Unquestionably, despite the previously analyzed results, there is a necessity for further research that arises, in order to investigate this technique across the spectrum of the polymeric materials and the microfluidic designs. Since this is a microfluidic product, it is also necessary to investigate long-term stability under various operational conditions. For this study to reach its potential in impact, future studies need to explore the scalability of this method for high-throughput manufacturing.

Evidently, the microelectrode bonding technology significantly advances the field of microfluidic chip fabrication, offering a pathway to more reliable and efficient devices that can meet the demands of commercial and research applications.

CRediT authorship contribution statement

Baishun Zhao: Conceptualization, Investigation, Writing – Original Draft, Writing - Review & Editing, **Wangqing Wu**: Conceptualization, Writing – Review & Editing., Funding acquisition, Resources. **Dimitrios Kontziampasis**: Writing - Review & Editing. **Lei Huang**: Data curation. **Bingyan Jiang**: Project administration, Funding acquisition, Resources.

Declaration of competing interest

The authors declare that they have no known competing financial interests or personal relationships that could have appeared to influence the work reported in this paper.

Acknowledgements

The authors acknowledge the financial support given by the National Natural Science Foundation of China (Key International (Regional) Joint Research Program (No. 51920105008), Normal project (No. 51875582), the Natural Science Foundation of Changsha municipality (No. kq2402215), the Huxiang Young Talents Program of Hunan Province (No. 2019RS2003), and the Open Research Fund of State Key Laboratory of Precision Manufacturing for Extreme Service Performance, Central South University, (No. ZZYJKT2023-11).

Data availability

All data included in this study are available upon request by contact with the corresponding author.

References

[1] E.K. Sackmann, A.L. Fulton, D.J. Beebe, The present and future role of microfluidics in biomedical research, Nature. 507 (2014) 181–189. https://doi.org/10.1038/nature13118.

[2] L. Jiao, Q. Xu, J. Tong, S. Liu, Y. Hu, Q. Guo, H. Wu, W. Li, Q. Zhao, R. Chen, Facile preparation of pliable

superamphiphobic papers with high and durable liquid repellency for anti-corrosion and open surface microfluidics, Appl. Surf. Sci. 606 (2022) 154845. https://doi.org/https://doi.org/10.1016/j.apsusc.2022.154845.

[3] H. Šípová-Jungová, L. Jurgová, E. Hemmerová, J. Homola, Interaction of Tris with DNA molecules and carboxylic groups on self-assembled monolayers of alkanethiols measured with surface plasmon resonance, Appl. Surf. Sci. 546 (2021) 148984. https://doi.org/https://doi.org/10.1016/j.apsusc.2021.148984.

[4] N.S. Bhise, J. Ribas, V. Manoharan, Y.S. Zhang, A. Polini, S. Massa, M.R. Dokmeci, A. Khademhosseini, Organ-on-a-chip platforms for studying drug delivery systems., J. Control. Release Off. J. Control. Release Soc. 190 (2014) 82–93. https://doi.org/10.1016/j.jconrel.2014.05.004.

[5] C. Dincer, R. Bruch, E. Costa-Rama, M.T. Fernandez-Abedu, A. Merkoci, A. Manz, G.A. Urban, F. Guder, Disposable Sensors in Diagnostics, Food, and Environmental Monitoring, Adv. Mater. 31 (2019). https://doi.org/10.1002/adma.201806739 WE - Science Citation Index Expanded (SCI-EXPANDED).

[6] D.T. Chiu, A.J. deMello, D. Di Carlo, P.S. Doyle, C. Hansen, R.M. Maceiczyk, R.C.R. Wootton, Small but Perfectly Formed? Successes, Challenges, and Opportunities for Microfluidics in the Chemical and Biological Sciences, Chem. 2 (2017) 201–223. https://doi.org/https://doi.org/10.1016/j.chempr.2017.01.009.

[7] E.B. Hua, Y. Zhang, K.Y. Yun, W.J. Pan, Y. Liu, S.X. Li, Y. Wang, R. Tu, M. Wang, Whole-Cell Biosensor and Producer Co-cultivation-Based Microfludic Platform for Screening *Saccharopolyspora erythraea* with Hyper, ACS Synth. Biol. (2022). https://doi.org/10.1021/acssynbio.2c00102.

[8] O.Z.- Chebotarev, High Throughput Microfluidic Platform Capable of Mimicking Key Vascular Microenvironments, University of Toronto (Canada), Ontario, Canada, 2013.

[9] H.W. Gao, C.L. Yan, W. Wu, J. Li, Application of Microfluidic Chip Technology in Food Safety Sensing, SENSORS. 20 (2020). https://doi.org/10.3390/s20061792.

[10] C.W. Tsao, Polymer microfluidics: Simple, low-cost fabrication process bridging academic lab research to commercialized production, Micromachines. 7 (2016). https://doi.org/10.3390/mi7120225.

[11] Y. Xu, Y.L. Ni, D.S. Li, Focus on the Microfludic Chip Papers in Chinese Journal of Analytical Chemistry in 2010, CHINESE J. Anal. Chem. 39 (2011) 1936–1939. https://doi.org/10.3724/SP.J.1096.2011.01936.

[12] T.A. Duncombe, A.M. Tentori, A.E. Herr, Microfluidics: reframing biological enquiry, Nat. Rev. Mol. Cell Biol. 16 (2015) 554–567. https://doi.org/10.1038/nrm4041.

[13] B. Liu, J. Cao, B. Hong, H. You, T. Li, Z. Yu, D. Li, B. Liang, N. Gan, A microfluidic chip platform based on Pt nanozyme and magnetized phage composite probes for dual-mode detecting and imaging pathogenic bacteria viability., Talanta. 275 (2024) 126067. https://doi.org/10.1016/j.talanta.2024.126067.

[14] G. Gharib, İ. Bütün, Z. Muganlı, G. Kozalak, İ. Namlı, S.S. Sarraf, V.E. Ahmadi, E. Toyran, A.J. van Wijnen, A. Koşar, Biomedical Applications of Microfluidic Devices: A Review, Biosensors. 12 (2022). https://doi.org/10.3390/bios12111023.

[15] P. Pattanayak, S.K. Singh, M. Gulati, S. Vishwas, B. Kapoor, D.K. Chellappan, K. Anand, G. Gupta, N.K. Jha, P.K. Gupta, P. Prasher, K. Dua, H. Dureja, D. Kumar, V. Kumar, Microfluidic chips: recent advances, critical strategies in design, applications and future perspectives, Microfluid. Nanofluidics. 25 (2021) 99. https://doi.org/10.1007/s10404-021-02502-2.

[16] R. Riahi, A. Tamayol, S.A.M. Shaegh, A.M. Ghaemmaghami, M.R. Dokmeci, A. Khademhosseini, Microfluidics for advanced drug delivery systems, Curr. Opin. Chem. Eng. 7 (2015) 101–112.

https://doi.org/https://doi.org/10.1016/j.coche.2014.12.001.

[17] N. Xiang, Z. Ni, Microfluidics for Biomedical Applications, Biosensors. 13 (2023). https://doi.org/10.3390/bios13020161.

[18] K. Giri, C.-W. Tsao, Recent Advances in Thermoplastic Microfluidic Bonding, Micromachines. 13 (2022). https://doi.org/10.3390/mi13030486.

[19] B. Zhao, Y. Qiang, W. Wu, B. Jiang, Tuning power ultrasound for enhanced performance of thermoplastic micro-injection molding: Principles, methods, and performances, Polymers (Basel). 13 (2021). https://doi.org/10.3390/polym13172877.

[20] P.N. Immanuel, C.-C. Chiang, C.-R. Yang, M. Subramani, T.-H. Lee, S.-J. Huang, Surface activation of poly(methyl methacrylate) for microfluidic device bonding through a H2O plasma treatment linked with a low-temperature annealing, J. Micromechanics Microengineering. 31 (2021) 55004. https://doi.org/10.1088/1361-6439/abf034.

[21] A. Shakeri, S. Khan, N.A. Jarad, T.F. Didar, The Fabrication and Bonding of Thermoplastic Microfluidics: A Review, Materials (Basel). 15 (2022). https://doi.org/10.3390/ma15186478.

[22] A. Welle, E. Gottwald, UV-Based Patterning of Polymeric Substrates for Cell Culture Applications, Biomed. Microdevices. 4 (2002) 33–41. https://doi.org/10.1023/A:1014267712144.

[23] R. Paoli, D. Di Giuseppe, M. Badiola-Mateos, E. Martinelli, M.J. Lopez-Martinez, J. Samitier, Rapid Manufacturing of Multilayered Microfluidic Devices for Organ on a Chip Applications, Sensors. 21 (2021). https://doi.org/10.3390/s21041382.

[24] N.X.T. Le, K.T.L. Trinh, N.Y. Lee, Poly(acrylic acid) as an adhesion promoter for UV-assisted thermoplastic bonding: Application for the in vitro construction of human blood vessels, Mater. Sci. Eng. C. 122 (2021) 111874. https://doi.org/https://doi.org/10.1016/j.msec.2021.111874.

[25] H.D. Lynh, C. Pin-Chuan, Novel solvent bonding method for creation of a three-dimensional, non-planar, hybrid PLA/PMMA microfluidic chip, Sensors Actuators A Phys. 280 (2018) 350–358. https://doi.org/https://doi.org/10.1016/j.sna.2018.08.002.

[26] H. Persson, S. Park, M. Mohan, K.K. Cheung, C.A. Simmons, E.W.K. Young, Rapid assembly of PMMA microfluidic devices with PETE membranes for studying the endothelium, Sensors Actuators B Chem. 356 (2022) 131342. https://doi.org/https://doi.org/10.1016/j.snb.2021.131342.

[27] B. Zhao, W. Wu, M. Zhou, B. Jiang, G. Ziegmann, Highly dynamic tempered in-mold thermocompression bonding of microfluidic chips: process characteristics and bonding performances, J. Mater. Res. Technol. 24 (2023) 639–652. https://doi.org/10.1016/j.jmrt.2023.03.040.

[28] G. Kulsharova, N. Dimov, M.P.C. Marques, N. Szita, F. Baganz, Simplified immobilisation method for histidine-tagged enzymes in poly(methyl methacrylate) microfluidic devices, N. Biotechnol. 47 (2018) 31–38. https://doi.org/https://doi.org/10.1016/j.nbt.2017.12.004.

[29] R. Sivakumar, N.Y. Lee, Microfluidic device fabrication mediated by surface chemical bonding, Analyst. 145 (2020) 4096–4110. https://doi.org/10.1039/d0an00614a.

[30] B. Acherjee, A.S. Kuar, S. Mitra, D. Misra, S. Acharyya, Experimental investigation on laser transmission welding of PMMA to ABS via response surface modeling, Opt. Laser Technol. 44 (2012) 1372–1383. https://doi.org/https://doi.org/10.1016/j.optlastec.2011.12.029.

[31] D. Podbiel, L. Boecking, H. Bott, J. Kassel, D. Czurratis, F. Laermer, R. Zengerle, J. Hoffmann, From CAD to microfluidic chip within one day: rapid prototyping of lab-on-chip cartridges using generic polymer parts, J. Micromechanics Microengineering. 30 (2020) 115012. https://doi.org/10.1088/1361-6439/aba5dd.

[32] K. Kistrup, C.E. Poulsen, M.F. Hansen, A. Wolff, Ultrasonic welding for fast bonding of self-aligned structures in lab-on-a-chip systems, Lab Chip. 15 (2015) 1998–2001. https://doi.org/10.1039/c5lc00174a.

[33] S.W. Li, J.H. Xu, Y.J. Wang, Y.C. Lu, G.S. Luo, Low-temperature bonding of poly-(methyl methacrylate) microfluidic devices under an ultrasonic field, J. Micromechanics Microengineering. 19 (2009) 15035. https://doi.org/10.1088/0960-1317/19/1/015035.

[34] K.F. Lei, S. Ahsan, N. Budraa, W.J. Li, J.D. Mai, Microwave bonding of polymer-based substrates for potential encapsulated micro/nanofluidic device fabrication, Sensors Actuators, A Phys. 114 (2004) 340–346. https://doi.org/10.1016/j.sna.2003.12.018.

[35] A.A. Yussuf, I. Sbarski, J.P. Hayes, M. Solomon, N. Tran, Microwave welding of polymeric-microfluidic devices, J. Micromechanics Microengineering. 15 (2005) 1692–1699. https://doi.org/10.1088/0960-1317/15/9/011.

[36] A.A. Yussuf, I. Sbarski, M. Solomon, N. Tran, J.P. Hayes, Sealing of polymeric-microfluidic devices by using high frequency electromagnetic field and screen printing technique, J. Mater. Process. Technol. 189 (2007) 401–408. https://doi.org/10.1016/j.jmatprotec.2007.02.013.

[37] S.R. Mahmoodi, P.-K. Sun, M. Mayer, R.S. Besser, Gas-assisted thermal bonding of thermoplastics for the fabrication of microfluidic devices, Microsyst. Technol. 25 (2019) 3923–3932. https://doi.org/10.1007/s00542-019-04380-9.

[38] P.M. Kristiansen, A. Karpik, J. Werder, M. Guilherme, M. Grob, Thermoplastic Microfluidics, Methods Mol. Biol. 2373 (2022) 39–55. https://doi.org/10.1007/978-1-0716-1693-2_3.

[39] A. Shakeri, N. Abu Jarad, S. Khan, T.F. Didar, Bio-functionalization of microfluidic platforms made of thermoplastic materials: A review, Anal. Chim. Acta. 1209 (2022). https://doi.org/10.1016/j.aca.2021.339283.

[40] K.T.L. Trinh, D.A. Thai, N.Y. Lee, Bonding Strategies for Thermoplastics Applicable for Bioanalysis and Diagnostics, MICROMACHINES. 13 (2022). https://doi.org/10.3390/mi13091503.

[41] C.W. Tsao, Polymer microfluidics: Simple, low-cost fabrication process bridging academic lab research to commercialized production, Micromachines. 7 (2016). https://doi.org/10.3390/mi7120225.

[42] M. Matteucci, A. Heiskanen, K. Zór, J. Emnéus, R. Taboryski, Comparison of Ultrasonic Welding and Thermal Bonding for the Integration of Thin Film Metal Electrodes in Injection Molded Polymeric Lab-on-Chip Systems for Electrochemistry, Sensors. 16 (2016). https://doi.org/10.3390/s16111795.

[43] B. Zhao, F. Mo, W. Wu, B. Jiang, G. Ziegmann, Deformation patterns and coordination mechanisms of cross-size microchannels during thermocompression bonding process, J. Mater. Res. Technol. 26 (2023) 3701–3709. https://doi.org/10.1016/j.jmrt.2023.08.141.

[44] C. Wei, H. Gu, Y.C. Gu, Y.H. Huang, D.X. Cheng, Z.Q. Li, L. Li, Abnormal interfacial bonding mechanisms of multi-material additive-manufactured tungsten-stainless steel sandwich structure, Int. J. Extrem. Manuf. 4 (2022). https://doi.org/10.1088/2631-7990/ac5f10.

[45] C. Wei, Z.Z. Zhang, D.X. Cheng, Z. Sun, M.H. Zhu, L. Li, An overview of laser-based multiple metallic material additive manufacturing: from macro- to micro-scales, Int. J. Extrem. Manuf. 3 (2021). https://doi.org/10.1088/2631-7990/abce04.

[46] A. Zolfaghari, T.T. Chen, A.Y. Yi, Additive manufacturing of precision optics at micro and nanoscale, Int. J. Extrem. Manuf. 1 (2019). https://doi.org/10.1088/2631-7990/ab0fa5.

[47] Z.Q. Fan, Q.Y. Tan, C.W. Kang, H. Huang, Advances and challenges in direct additive manufacturing of dense ceramic oxides, Int. J. Extrem. Manuf. 6 (2024). https://doi.org/10.1088/2631-7990/ad5424.

[48] C.J. Shuai, D.S. Li, X. Yao, X. Li, C.D. Gao, Additive manufacturing of promising heterostructure for biomedical applications, Int. J. Extrem. Manuf. 5 (2023). https://doi.org/10.1088/2631-7990/acded2.

[49] X.R. Li, B.Y. Zhang, T. Jakobi, Z.L. Yu, L.Q. Ren, Z.H. Zhang, Laser-based bionic manufacturing, Int. J. Extrem. Manuf. 6 (2024). https://doi.org/10.1088/2631-7990/ad3f59.

[50] J.S. Wang, F.Z. Fang, H.J. An, S. Wu, H.M. Qi, Y.X. Cai, G.Y. Guo, Laser machining fundamentals: micro, nano, atomic and close-to-atomic scales, Int. J. Extrem. Manuf. 5 (2023). https://doi.org/10.1088/2631-7990/acb134.

[51] X.L. Wang, D.T.T. Phan, D. Zhao, S.C. George, C.C.W. Hughes, A.P. Lee, An on-chip microfluidic pressure regulator that facilitates reproducible loading of cells and hydrogels into microphysiological system platforms, Lab Chip. 16 (2016) 868–876. https://doi.org/10.1039/c5lc01563d.

[52] S.Q. Hu, X. Huan, Y. Liu, S.X. Cao, Z.R. Wang, J.T. Kim, Recent advances in meniscus-on-demand three-dimensional micro- and nano-printing for electronics and photonics, Int. J. Extrem. Manuf. 5 (2023). https://doi.org/10.1088/2631-7990/acdf2d.

[53] J.M. Castro, S. Rajaraman, Experimental and Modeling Based Investigations of Process Parameters on a Novel, 3D Printed and Self-Insulated 24-Well, High-Throughput 3D Microelectrode Array Device for Biological Applications, J. MICROELECTROMECHANICAL Syst. 31 (2022) 358–371. https://doi.org/10.1109/JMEMS.2022.3160663.

[54] A. Kundu, A. Rozman, S. Rajaraman, Development of a 3D Printed, Self-Insulated, High-Throughput 3D Microelectrode Array (HT-3DMEA), J. MICROELECTROMECHANICAL Syst. 29 (2020) 1091–1093. https://doi.org/10.1109/JMEMS.2020.3003644.

[55] A. Kundu, L. McCoy, N. Azim, H. Nguyen, C.M. Didier, T. Ausaf, A.D. Sharma, J.L. Curley, M.J. Moore, S. Rajaraman, Fabrication and Characterization of 3D Printed, 3D Microelectrode Arrays for Interfacing with a Peripheral Nerve-on-a-Chip, ACS Biomater. Sci. Eng. 7 (2021) 3018–3029. https://doi.org/10.1021/acsbiomaterials.0c01184.

[56] T.N.A. Vo, P.-C. Chen, Maximizing interfacial bonding strength between PDMS and PMMA substrates for manufacturing hybrid microfluidic devices withstanding extremely high flow rate and high operation pressure, Sensors Actuators A Phys. 334 (2022) 113330. https://doi.org/https://doi.org/10.1016/j.sna.2021.113330.

[57] M. Madadi, A. Madadi, R. Zareifar, A. Nikfarjam, A simple solvent-assisted method for thermal bonding of large-surface, multilayer PMMA microfluidic devices, Sensors Actuators A Phys. 349 (2023) 114077. https://doi.org/https://doi.org/10.1016/j.sna.2022.114077.

[58] T. Guan, S. Yuket, H. Cong, D.W. Carton, N. Zhang, Permanent Hydrophobic Surface Treatment Combined with Solvent Vapor-Assisted Thermal Bonding for Mass Production of Cyclic Olefin Copolymer Microfluidic Chips, ACS Omega. 7 (2022) 20104–20117. https://doi.org/10.1021/acsomega.2c01948.

[59] M. Busek, S. Nøvik, A. Aizenshtadt, M. Amirola-Martinez, T. Combriat, S. Grünzner, S. Krauss, Thermoplastic Elastomer (TPE)–Poly(Methyl Methacrylate) (PMMA) Hybrid Devices for Active Pumping PDMS-Free Organ-on-a-Chip Systems, Biosensors. 11 (2021). https://doi.org/10.3390/bios11050162.

[60] J. Cheon, S. Kim, Intermediate layer-based bonding techniques for polydimethylsiloxane/digital light processing 3D-printed microfluidic devices, J. Micromechanics Microengineering. 29 (2019) 95005. https://doi.org/10.1088/1361-6439/ab27d3.
[61] X. Ku, G. Zhuang, G. Li, A universal approach for irreversible bonding of rigid substrate-based microfluidic devices at room temperature, Microfluid. Nanofluidics. 22 (2018) 17. https://doi.org/10.1007/s10404-018-2039-3.
[62] N. Ling, J.S. Lee, N.Y. Lee, Solvent-assisted low-temperature and low-pressure poly(methylmethacrylate) bonding coupled with selective microchannel hydrophobic coating for reliable sealing, Sensors Actuators A Phys. 265 (2017) 168–173. https://doi.org/https://doi.org/10.1016/j.sna.2017.08.023.
[63] A. Bamshad, A. Nikfarjam, H. Khaleghi, A new simple and fast thermally-solvent assisted method to bond PMMA–PMMA in micro-fluidics devices, J. Micromechanics Microengineering. 26 (2016) 65017. https://doi.org/10.1088/0960-1317/26/6/065017.
[64] S. Hassanpour-Tamrin, A. Sanati-Nezhad, A. Sen, A simple and low-cost approach for irreversible bonding of polymethylmethacrylate and polydimethylsiloxane at room temperature for high-pressure hybrid microfluidics, Sci. Rep. 11 (2021) 4821. https://doi.org/10.1038/s41598-021-83011-8.
[65] B. Zhao, W. Wu, B. Jiang, The in-mold thermocompression bonding process of microfluidic chips based on the highly dynamic variotherm technology: Process characteristics, in: NanoMan 2022 AETS 2022 - 2022 8th Int. Conf. Nanomanufacturing 4th AET Symp. ACSM Digit. Manuf., 2022: pp. 1–6. https://doi.org/10.1109/Nanoman-AETS56035.2022.10119480.